nature physics

SUPPLEMENTARY INFORMATION

https://doi.org/10.1038/s41567-018-0129-5

In the format provided by the authors and unedited.

Observation of two types of fractional excitation in the Kitaev honeycomb magnet

Nejc Janša[1], Andrej Zorko[1], Matjaž Gomilšek[1], Matej Pregelj[1], Karl W. Krämer[2], Daniel Biner[2], Alun Biffin[3], Christian Rüegg[3,4] and Martin Klanjšek[1]*

[1]Jožef Stefan Institute, Ljubljana, Slovenia. [2]Department of Chemistry and Biochemistry, University of Bern, Bern, Switzerland. [3]Laboratory for Neutron Scattering and Imaging, Paul Scherrer Institut, Villigen, Switzerland. [4]Department of Quantum Matter Physics, University of Geneva, Geneva, Switzerland. *e-mail: martin.klanjsek@ijs.si

SUPPLEMENTARY INFORMATION

to "Observation of two types of fractional excitations in the Kitaev honeycomb magnet" by Nejc Janša *et al.*

Magnetic susceptibility

Magnetic susceptibility measurements of α-$RuCl_3$ were performed using a Quantum Design MPMS. A powdered sample of the mass 22.5 mg was placed into a plastic capsule, in a glovebox to avoid contact with air, and then quickly transferred into the MPMS. Fig. S1 shows the measured susceptibility taken with cooling in field and in zero field. The obtained curve with the magnetic transition at $T_{N2} = 14$ K (inset of Fig. S1) is almost identical to the corresponding curve in Ref. [S1].

Nuclear magnetic resonance

Orientation dependence of the NMR spectrum. The ^{35}Cl nuclear magnetic resonance (NMR) spectra were recorded point by point in frequency steps of 50 or 100 kHz, so that the Fourier transform of the signal was integrated at each step to arrive at the individual spectral point. The covered NMR frequency range was from 34 MHz, the lower limit of our setup, up to 50 MHz. The dependence of the corresponding part of the NMR spectrum on the direction of the external magnetic field of 9.4 T (described by the angle ϑ from the crystal ab plane) at a temperature of 20 K is shown in Fig. S2. The spectra are extremely broad because of a large ^{35}Cl (with $I = 3/2$ spin) quadrupole interaction. As concluded in Methods, a large portion of the covered frequency range is associated with the central, $1/2 \longleftrightarrow -1/2$ ^{35}Cl NMR transition. As this transition is observed to consist of at least three peaks (Fig. S2), even for the symmetric $\vartheta = 90°$ orientation, while there are only two inequivalent Cl sites in the crystal structure, the splitting of the central line is likely a consequence of stacking faults in the layered crystal structure or crystal twinning, or both.

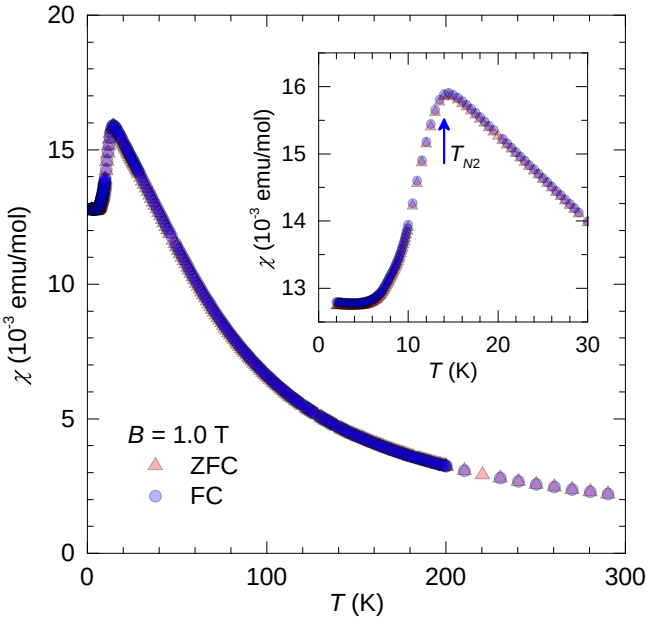

FIG. S1: **Magnetic susceptibility.** Zero-field-cooled (ZFC) and field-cooled (FC) magnetic susceptibility of the powdered α-$RuCl_3$ sample in a magnetic field of 1.0 T. Inset is a blow-up around the magnetic phase transition at $T_{N2} = 14$ K.

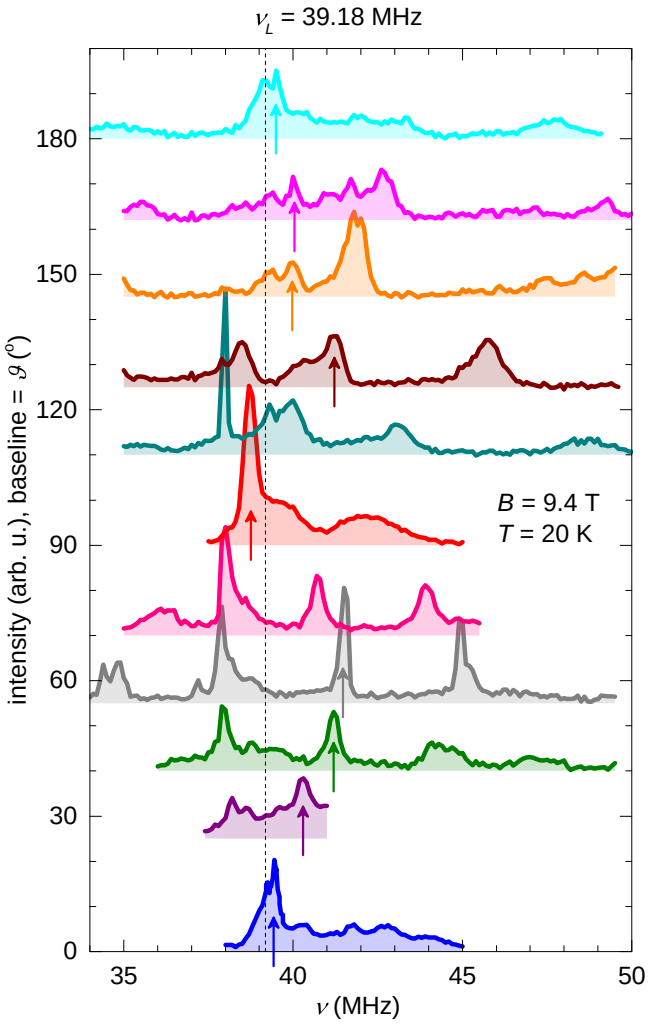

FIG. S2: **Orientation dependence of the NMR spectrum.** Central line of the ^{35}Cl NMR spectrum of the α-$RuCl_3$ single crystal taken at 20 K in the field of 9.4 T applied at an angle ϑ with respect to the crystal ab plane (as shown in Fig. 1a). The plane of rotation is at an angle of 15° from the crystal b axis (as shown in Fig. 1a). Dashed vertical line indicates the Larmor frequency ν_L. Arrows mark the peak whose temperature dependence is analyzed in Fig. S3 and where T_1 displayed in Fig. 3 was measured. The $\vartheta = 180°$ spectrum corresponds to the only field direction outside the red fan in Fig. 1a.

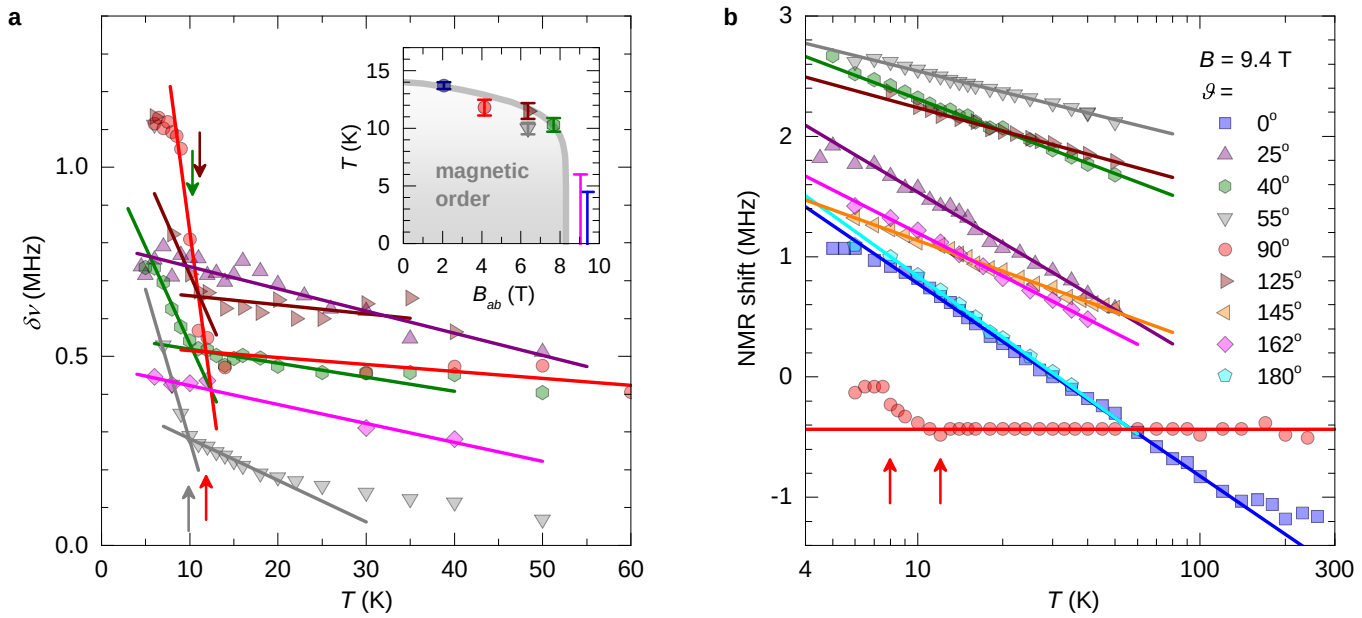

FIG. S3: **Temperature dependence of the NMR line.** The temperature (T) dependence of **a**, the width $\delta\nu$, and **b**, the NMR shift of dominant ^{35}Cl NMR peaks (marked by arrows in Fig. S2) in 9.4 T ($\nu_L = 39.18$ MHz for ^{35}Cl) for various sample orientations given by ϑ. The overlaping peaks for some values of ϑ do not allow the determination of $\delta\nu$. For each dataset drawn in **a**, straight lines are linear fits on both sides of the kink at T_{N2} (determined as the temperature of intersection and marked by an arrow) indicating the onset of low-temperature magnetic ordering. Inset shows the obtained points of the phase boundary (same symbols as the corresponding $\delta\nu(T)$ datasets) compared to the result of Ref. [S1] (gray line). Straight lines in **b** are phenomenological $\log T$ fits. Only the $\vartheta = 90°$ dataset in **b** shows signs of magnetic transitions (marked by arrows).

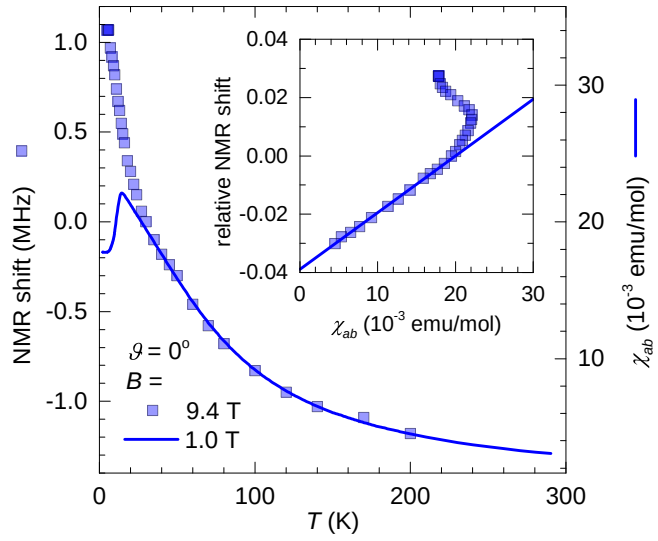

FIG. S4: **NMR shift against susceptibility.** Temperature dependencies of the ^{35}Cl NMR shift of the dominant NMR peak measured in 9.4 T with the field in the ab plane ($\vartheta = 0°$) and magnetic susceptibility χ_{ab} are proportional to each other down to 35 K. Inset shows the dependence of the relative NMR shift (i.e., NMR shift divided by $\nu_L = 39.18$ MHz) on χ_{ab}. Line is a linear fit of the dataset up to $20 \cdot 10^{-3}$ emu/mol, i.e., down to 35 K, leading to the component $A = 1.35$ T (in the ab plane) of the hyperfine coupling tensor between ^{35}Cl and the Ru^{3+} $S = 1/2$ spin, as described in Methods.

Temperature dependence of the NMR line. We measured the temperature dependence of the dominant ^{35}Cl NMR peak in a field of 9.4 T for various sample orientations with respect to the magnetic field direction. From these measurements, we determined the temperature dependence of the frequency width (Fig. S3a) and the NMR shift of the peak with respect to the Larmor frequency (Fig. S3b). For $B_{ab} < 8$ T, the width exhibits a clear kink as a function of temperature, which indicates the onset of NMR line broadening at the phase transition into the magnetically ordered state. Plotting the temperature of the kink as a function of B_{ab} in the inset of Fig. S3 (and in Fig. 1b), we obtain the phase boundary of the magnetically ordered state, which perfectly matches the result of the reference study [S1]. In contrast, the NMR shift does not exhibit any signs of a magnetic transition, except for the $\vartheta = 90°$ dataset. We find the NMR shift to be a monotonic function of temperature T, empirically following a $\log T$ dependence over a broad temperature range.

Contributions to the NMR shift. Fig. S4 shows the temperature dependence of the frequency shift of the dominant NMR peak taken in 9.4 T for $\vartheta = 0°$ (Fig. S3b), i.e., with the field in the ab plane. Its comparison to the rescaled magnetic susceptibility χ_{ab} allows us to separate the magnetic contribution to the NMR shift from the temperature-independent quadrupole contribution.

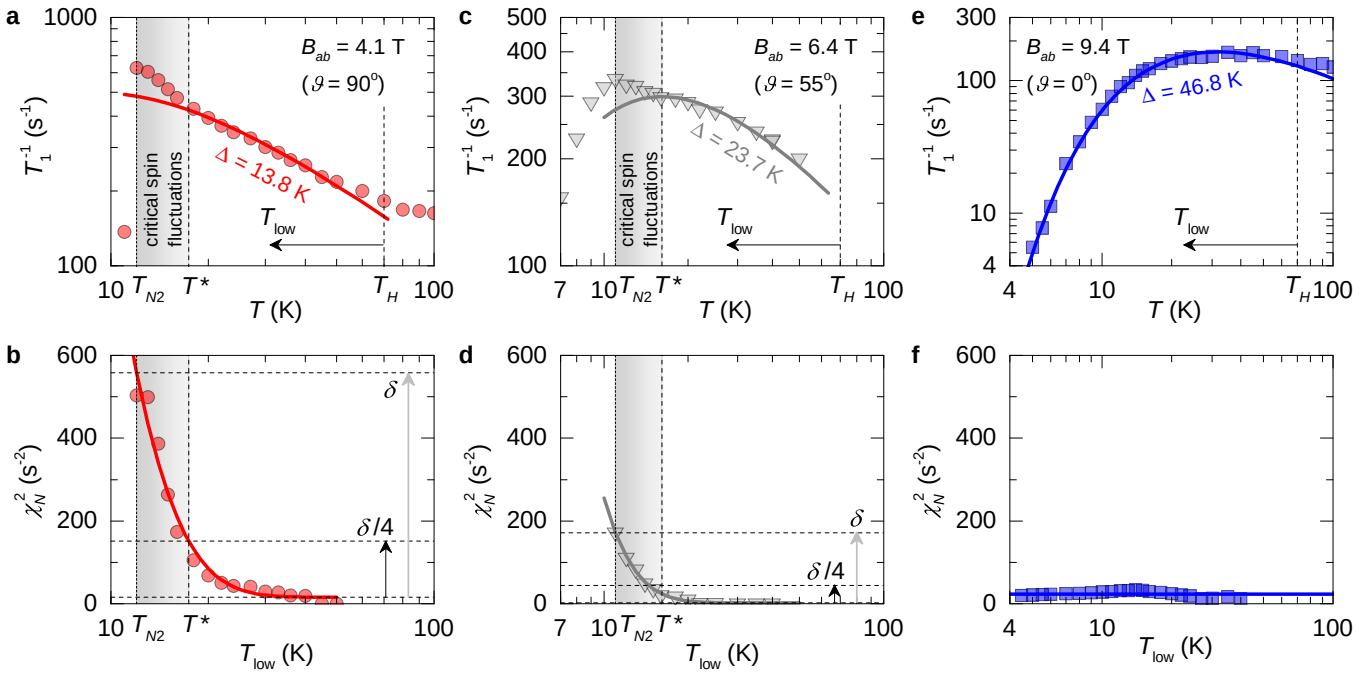

FIG. S5: **Determination of the onset temperature T^* for the critical spin fluctuations. a,c,e**, The representative ^{35}Cl $T_1^{-1}(T)$ datasets from Fig. 3 taken in 9.4 T for $\vartheta = 90°$, 55° and 0°. Solid lines are fits to Eq. (1) with $n = 0.67$ in the temperature range between T^*, where the critical spin fluctuations (gray) related to magnetic ordering at T_{N2} vanish, and $T_H \approx 70$ K. **b,d,f**, The $T_1^{-1}(T)$ datasets in **a**, **c** and **e** are fitted with Eq. (1) in the temperature range between the varying $T_{\rm low} < T_H$ and T_H (so that the fitting range contains at least three data points), and the goodness of the fit χ^2_N (normalized to the number N of involved data points) is plotted as a function of $T_{\rm low}$. Solid lines are fits with the phenomenological function $\chi^2_N = a\exp(-\kappa T_{\rm low}) + b$. T^* is defined as the temperature where the χ^2_N fit (measured from the base line) reaches 1/4 of the maximum value δ reached at T_{N2}. The dataset for $\vartheta = 0°$ exhibits no magnetic ordering (**e**) and thus no critical spin fluctuations (**f**).

Determination of the onset temperature T^*. To determine the onset temperature T^* for the critical spin fluctuations preceding the magnetic ordering at T_{N2}, we apply the following procedure to the selected $T_1^{-1}(T)$ dataset. We fit a part of the dataset between $T_H = 0.375J_K \approx 70$ K (for $J_K = 190$ K [S4]) and the varying temperature $T_{\rm low} < T_H$, which contains at least three data points, to Eq. (1) with $n = 0.67$ for Kitaev spin fluctuations. Then we plot the goodness of the fit χ^2_N (normalized to the number N of involved data points) as a function of $T_{\rm low}$. As shown in Fig. S5 for the representative ^{35}Cl $T_1^{-1}(T)$ datasets from Fig. 3, χ^2_N is almost constant down to some temperature, and then starts to rapidly increase as $T_{\rm low}$ approaches the magnetic ordering temperature T_{N2}. This rise indicates that the fitting range starts to progressively cover the data points that do not follow Eq. (1) anymore, meaning that they already reflect the critical spin fluctuations preceding the magnetic ordering at T_{N2}. The $\chi^2_N(T_{\rm low})$ datasets can be nicely fitted to a phenomenological function $\chi^2_N = a\exp(-\kappa T_{\rm low}) + b$ where a, b and κ are the fitting parameters. We define T^* as the temperature where the χ^2_N fit (measured from the base line) reaches 1/4 of the maximum value reached at T_{N2}, as shown in Figs. S5b and d. Comparing Figs. S5b, d and f, we see that the critical spin fluctuations weaken with increasing B_{ab}, i.e., when moving towards the critical magnetic field $B_c \approx 8$ T in the phase diagram in Fig. 1b, and disappear above B_c, just as expected.

Gap value across the NMR spectrum. As the values of the hyperfine coupling constant A are different for different NMR peaks, T_1^{-1}, which is proportional to A^2, is expected to vary across the NMR spectrum. The question then arises whether there is any variation of the determined spin-excitation gap Δ across the NMR spectrum. Fig. S6 shows the determination of Δ on various ^{35}Cl NMR peaks for selected orientations ϑ in 9.4 T. Although the $T_1^{-1}(T)$ datasets taken on different peaks are significantly offset with respect to each other on the logarithmic scale, as expected, the obtained Δ shows only a negligible variation across the NMR spectrum. This is actually expected, as Δ is related only to the underlying Kitaev physics and should not depend on the coupling constants.

Choice of the g-tensor eigenvalues. While there is a consensus regarding the value of $g_{ab} = 2.5$ in the lit-

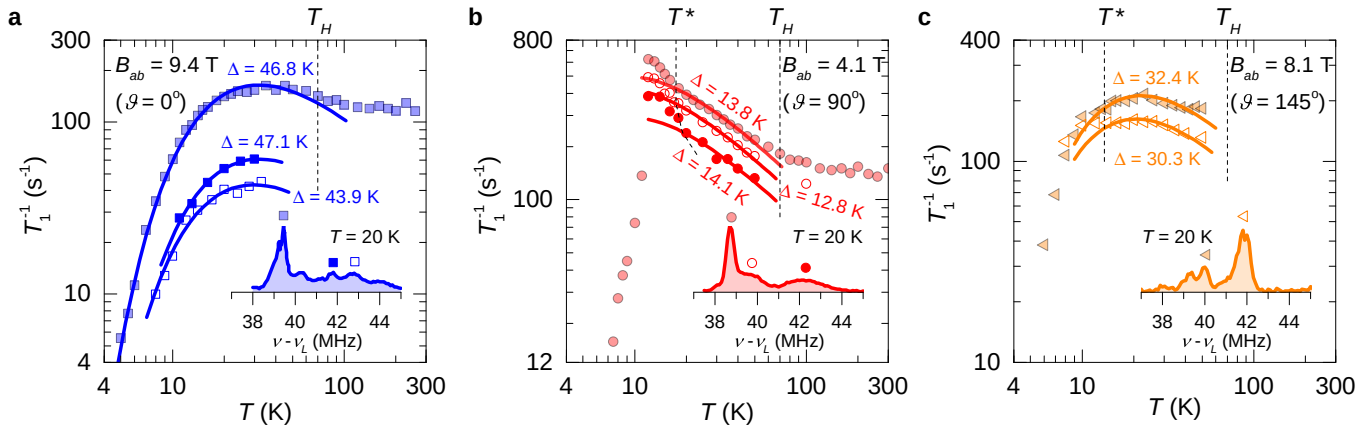

FIG. S6: **Gap values on different NMR peaks. a-c**, The $T_1^{-1}(T)$ datasets taken on different ^{35}Cl NMR peaks (marked with the corresponding symbols in the insets, which show the NMR spectra) in 9.4 T for selected orientations ϑ (and hence B_{ab}). To obtain the gap value Δ for different NMR peaks, each dataset is fitted with Eq. (1) between T^*, determined as shown in Fig. S5, and $T_H = 70$ K.

erature [S2, S3], the value of g_{c^*} was first estimated to 0.4 in Ref. [S2] and then refined to 1.1 in Ref. [S3] based on theoretical calculations. As the theoretical result also fits perfectly to the magnetization curves from Ref. [S1], the corresponding g_{c^*} value is definitely more reliable. Nevertheless, to see the dependence of our conclusions on the choice of the g_{c^*} value, we repeat the analysis of the field dependence of the spin-excitation gap Δ from Fig. 1c, where we assumed $g_{c^*} = 1.1$, also with the alternative value $g_{c^*} = 0.4$. As shown in Fig. S7, the two datasets differ only a little, so that the obtained values $J_K = 183$ K and 212 K of the Kitaev exchange coupling are both in agreement with the recent determination of $J_K = 190$ K in Ref. [S4]. Our conclusions are thus essentially independent of the choice of the g_{c^*} value.

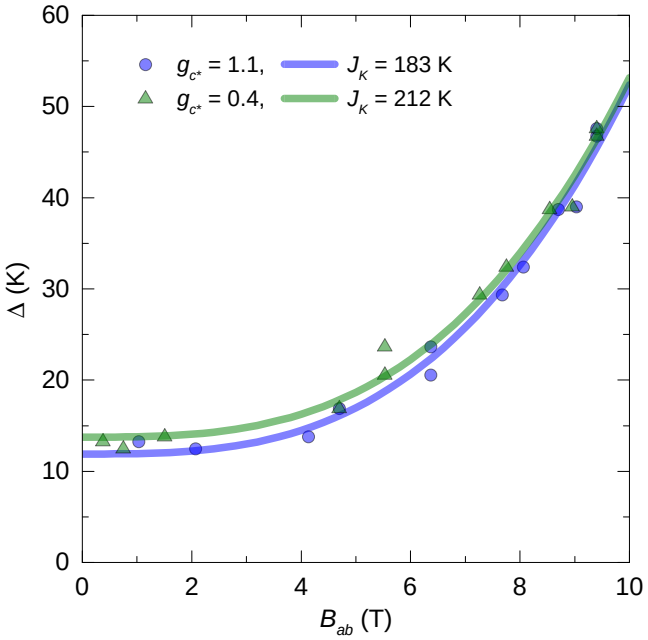

FIG. S7: **Choice of the g_{c^*} value.** The spin-excitation gap Δ as a function of B_{ab} for two different choices of g_{c^*}. The choice $g_{c^*} = 1.1$ is used in the main text. Solid lines are fits with Eq. (2).

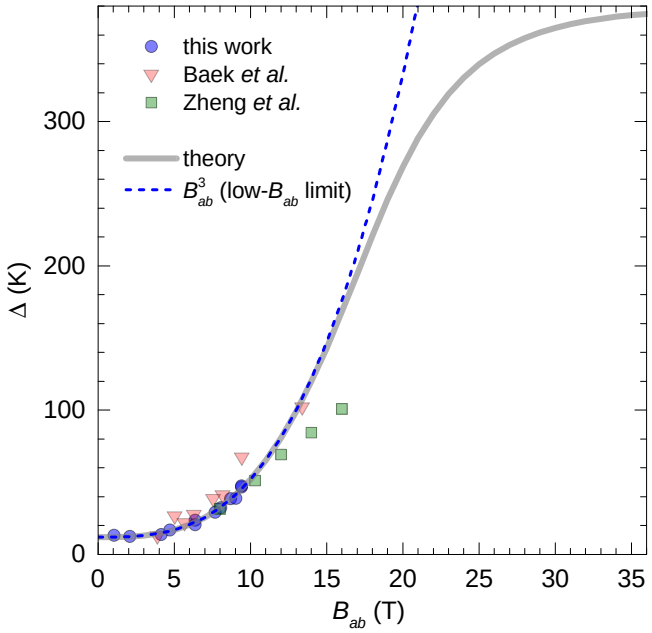

FIG. S8: **Spin-excitation gap.** The spin-excitation gap Δ as a function of the magnetic field B_{ab} obtained from $T_1^{-1}(T)$ data in our work and in two recent works [S5, S6] using our model given by Eq. (1). The data are compared to the full theoretical expression described in Methods (using $J_K = 183$ K determined in Fig. 1c, $\alpha = 1.2$, $g = g_{ab}$), which simplifies to the B_{ab}^3 dependence given by Eq. (2) (i.e., Δ_0 added to Δ_f in Eq. (13)) in the low-field region.

Comparison with recent works

Recent NMR measurements. Very recently, two ^{35}Cl NMR studies of α-$RuCl_3$ appeared [S5, S6]. The analysis of both studies is focused on the low-temperature region below 15 K. Using a simple exponential model $T_1^{-1} \propto \exp(-\Delta_s/T)$ in this region, Ref. [S5] finds that the spin-excitation gap Δ_s opens linearly with the field above the critical field of around 10 T. On the other hand, Ref. [S6] extends the covered temperature range down to 1.5 K and finds a low-temperature gapless, power-law behavior of $T_1^{-1}(T)$ in the covered high-field region above the critical field of around 8 T.

As these conclusions are very different from our own, also because of a quite different data analysis, we reanalyze the $T_1^{-1}(T)$ datasets obtained in these two works also with our theoretically verified model given by Eq. (1). As in our work, we focus on the Kitaev paramagnetic region, i.e., on the temperature range from $T_H = 70$ K down to the onset of critical fluctuations related to magnetic ordering below 8 T, and down to 4.2 K above 8 T (or a bit higher at higher fields), including the characteristic maximum in $T_1^{-1}(T)$ as the main feature. The data in Ref. [S6] were taken with a field applied in the crystal ab plane, while the data in Ref. [S5] were taken with a field applied at 30° and −60° with respect to the ab plane. In this case, we calculate the effective field values B_{ab} in the same way as in our work. The obtained field dependence of the excitation gap $\Delta(B_{ab})$ for both works is shown in Fig. S8 together with our result. Applying our analysis to the data from all three works apparently leads to relatively consistent results. Nevertheless, the results for the data from Refs. [S5, S6] alone do not allow us to make any conclusions about the cubic field dependence of Δ, mostly due to the lack of important low-field data points. Regarding Ref. [S6], the obtained $\Delta(B_{ab})$ data points, which complement our field region, nicely continue the trend set by our data points. The obtained trend is approximately linear in field, consistent with the theoretical prediction in this intermediate-field region, although with a different slope. As the theoretical prediction is based on a perturbative treatment, it is not surprising that it might not give reliable results outside the low-field region.

In light of our conclusions, the reported findings of these two works should be understood in the following way. While the true signs of fractionalization into Majorana fermions and gauge fluxes can be found in the Kitaev paramagnetic region covering a broad temperature range up to around 100 K (Fig. 1b), the physics at low temperatures of the order of 10 K and below is apparently obscured by the effect of inevitable non-Kitaev interactions, as predicted already in Ref. [S6].

Recent specific-heat measurements. The magnetic field dependence of the spin-excitation gap was recently determined also from the temperature dependence of the specific heat above the critical magnetic field of around 8 T [S7]. Using a simple exponential model $C_m \propto \exp(-\Delta_{\mathrm{Sears}}/T)$ for the magnetic contribution to the specific heat C_m in the low-temperature region, the authors concluded on a linear opening of the gap Δ_{Sears} with the field B_{ab} above the critical field, in an attempt to show the consistency with the $d = 2$ Ising model. However, a careful look at the $\Delta_{\mathrm{Sears}}(B_{ab})$ dataset, shown in Fig. S9, reveals a clear convex shape, which can be nicely fitted with the cubic B_{ab}^3 dependence with a finite zero-field value, in accordance with Eq. (2). As the Δ_{Sears} values in Ref. [S7] were obtained using a simple fitting model different from our theoretically verified model in Eq. (1), this result cannot be directly compared to our own $\Delta(B_{ab})$ dataset from Fig. 1c. For the purpose of comparison, we rescale the $\Delta_{\mathrm{Sears}}(B_{ab})$ dataset in Fig. S9 to match our $\Delta(B_{ab})$ dataset at 9 T. The datasets can then be considered consistent with each other, where the B_{ab}^3 fits of both yield consistent zero-field values.

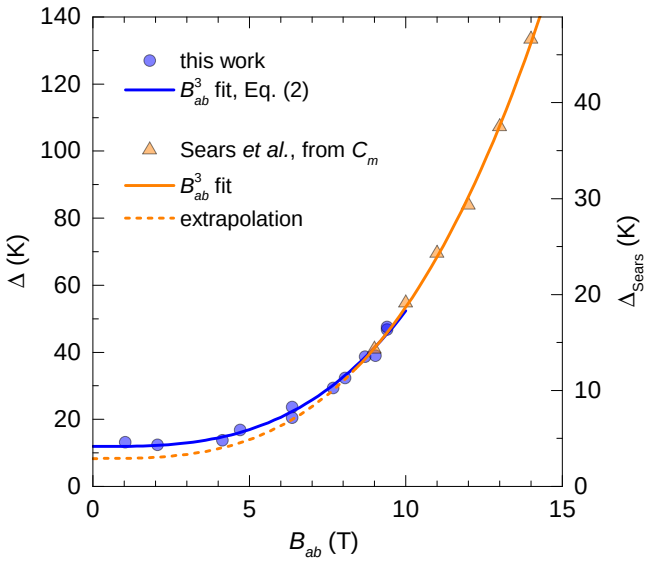

FIG. S9: **Spin-excitation gap from the specific heat.** The spin-excitation gap Δ as a function of the magnetic field B_{ab} from Fig. 1c compared to the $\Delta(B_{ab})$ dataset obtained from the specific-heat measurements in Ref. [S7] (scale Δ_{Sears} on the right vertical axis) rescaled to match our dataset at 9 T (scale Δ on the left vertical axis). Blue line is a theoretical B_{ab}^3 curve given by Eq. (2) (using $J_K = 183$ K determined in Fig. 1c, $\alpha = 1.2$, $g = g_{ab}$), solid orange line is a B_{ab}^3 fit of the specific-heat $\Delta(B_{ab})$ dataset and dashed orange line is its extrapolation to the low-field region.

[S1] R. D. Johnson, S. C. Williams, A. A. Haghighirad, J. Singleton, V. Zapf, P. Manuel, I. I. Mazin, Y. Li, H. O. Jeschke, R. Valentí, and R. Coldea, Monoclinic crystal

structure of α-$RuCl_3$ and the zigzag antiferromagnetic ground state, *Phys. Rev. B* **92**, 235119 (2015).

[S2] Y. Kubota, H. Tanaka, T. Ono, Y. Narumi, and K. Kindo, Successive magnetic phase transitions in α-$RuCl_3$: XY-like frustrated magnet on the honeycomb lattice, *Phys. Rev. B* **91**, 094422 (2015).

[S3] R. Yadav, N. A. Bogdanov, V. M. Katukuri, S. Nishimoto, J. van den Brink, and L. Hozoi, Kitaev exchange and field-induced quantum spin-liquid states in honeycomb α-$RuCl_3$, *Sci. Rep.* **6**, 37925 (2016).

[S4] S.-H. Do, S.-Y. Park, J. Yoshitake, J. Nasu, Y. Motome, Y. S. Kwon, D. T. Adroja, D. J. Voneshen, K. Kim, T.-H. Jang, J.-H. Park, K.-Y. Choi, and S. Ji, Majorana fermions in the Kitaev quantum spin system α-$RuCl_3$, *Nature Phys.* **13**, 1079 (2017).

[S5] S.-H. Baek, S.-H. Do, K.-Y. Choi, Y. S. Kwon, A. U. B. Wolter, S. Nishimoto, J. van den Brink, and B. Büchner, Evidence for a Field-induced Quantum Spin Liquid in α-$RuCl_3$, *Phys. Rev. Lett.* **119**, 037201 (2017).

[S6] J. Zheng, K. Ran, T. Li, J. Wang, P. Wang, B. Liu, Z.-X. Liu, B. Normand, J. Wen, and W. Yu, Gapless Spin Excitations in the Field-Induced Quantum Spin Liquid Phase of α-$RuCl_3$, *Phys. Rev. Lett.* **119**, 227208 (2017).

[S7] J. A. Sears, Y. Zhao, Z. Xu, J. W. Lynn, and Y.-J. Kim, Phase diagram of α-$RuCl_3$ in an in-plane magnetic field, *Phys. Rev. B* **95**, 180411(R) (2017).